On a flexible multibody modelling approach using FE-based contact formulation for describing gear transmission error

Youness Benaicha, Joël Perret-Liaudet, Jean-Daniel Beley, Emmanuel Rigaud, Fabrice Thouverez

On a flexible multibody modelling approach using FE-based contact formulation for describing gear transmission error

Y. Benaïcha[a,b,*], J. Perret-Liaudet[a], J-D. Beley[b], E. Rigaud[a] and F. Thouverez[a]

[a]Univ Lyon, Ecole Centrale de Lyon, ENISE, ENTPE, CNRS, Laboratoire de Tribologie et Dynamique des Systèmes LTDS, UMR 5513, F-69134, Ecully, France

[b]ANSYS SAS, 35-37 rue Louis Guérin, 69100 Villeurbanne Cedex, France

ARTICLE INFO

Keywords:
Gear transmission error
Flexible multibody modelling
Manufacturing errors
Time varying mesh stiffness
Contact Formulation

ABSTRACT

This paper provides an insight into the efficiency and accuracy of a multibody approach to model gear transmission error. The multibody model is based on an augmented Lagrangian contact formulation considering a surface-to-surface contact detection. The case of spur and helical gears transmitting power between parallel shafts is considered. The static transmission error is computed without any assumptions about the contact lines positions and orientations. Tooth and wheel body flexibility and tooth profile deviations are taken into account. The main objective of this study is to evaluate the efficiency and possibilities of the proposed methodology. To this end, the static transmission error is benchmarked against the results obtained from a classical approach which is based on the computation of the equation describing the static equilibrium of the gear pair for a set of successive positions of the driving wheel.

1. Introduction

Noise, vibration and harshness (NVH) prediction is one of the main items in the specifications of gear transmission systems. Generally, the whining noise constitutes the dominant source of noise [6, 32, 39, 57]. This structure-borne noise results from the dynamic mesh force, corresponding to the time varying normal contact force. Vibrations propagate through the gear wheel bodies, the shafts and the bearings to the housing. The vibratory state of the latter is responsible for the radiated noise [6, 32]. For example, in the transportation industry, the whining noise corresponds to a large part of the noise perceived by passengers as well as the noise perceived outside the vehicle. In this context, one common goal to improve NVH is to obtain quiet gear systems by reducing the whining noise level. The dynamic mesh force results mainly from the well-known static transmission error (STE) defined as the difference between the actual position of the output gear and the position it would occupy if the gear pair were perfectly conjugate [17, 57]. The STE is expressed along the line of action as:

$$\delta(\theta_1) = R_{b2}\theta_2 - R_{b1}\theta_1 \tag{1}$$

θ_1 and θ_2 are respectively the angular position of the input wheel and the output gear. R_{b1} and R_{b2} are the base radii of the input wheel and the output gear. The gear dynamics induced by the STE remains complex to model as difficulties stem from the two following main reasons. The first one corresponds to the different space scales involved in the gear modelling [52, 13]. The second reason concerns the coupling between the global behaviour of the whole transmission and the local behaviour at the gear mesh [24]. As a first necessary step, many studies focus on the optimization of gear macro and micro-geometries to reduce unintended vibroacoustic phenomena [5, 14, 28, 29, 44, 49, 56] but noise reduction remains a challenge. The accurate estimation of the STE is still a major task for the NVH prediction of geared transmissions.

The static transmission error and the mesh contact force distribution along the contact line strongly depend on manufacturing errors (eccentricity, pitch error, profile error), micro-geometry deviation (longitudinal crowning, profile correction) [17, 24, 21, 65], tooth deformation (hertzian contact, tooth bending and shearing), and global deformations which induce shafts misalignment [47]). Manufacturing errors and micro-geometry deviation influence deeply the dynamic characteristics and they can be used to counterbalance the effect of the gear pair deformation [2, 3, 26, 36, 38, 42].

*Corresponding author
youness.benaicha@ec-lyon.fr (Y. Benaïcha)
ORCID(s):

Nomenclature

Matrices and vectors

$\mathbf{1}$	Unity column vector
$\mathbf{e}(\theta_1)$	Initial gap vector
$\mathbf{x}$	Vector of generalized displacements
$\mathbf{p}(\theta_1)$	Distributed load
$\mathbf{C}$	Damping matrix
$\mathbf{H}(\theta_1)$	Symmetric semi-positive compliance matrix
$\mathbf{K}$	Stiffness matrix
$\mathbf{M}$	Mass matrix
$\mathbf{F}_{ext}$	Vector of external force
$\mathbf{F}_{nl}$	Vector of nonlinear force

Scalars

α	Pressure angle
$\delta(\theta_1)$	Static transmission error
ϵ_α	Contact ratio
ϵ_t	Total contact ratio
κ	Mathematical stiffness coefficient
λ	Lagrange multiplier
τ	Maximum shear stress
$k(\theta_1)$	Mesh stiffness
m_n	Gear module
a'	Center distance
b_f	Face width
b_w	Rim width
h	Contact width
h_a	Addendum
h_f	Dedendum
r_H	Radius of holes
r_S	Starting radius of tip relief modification
x	Profile shift coefficient
z_0	Contact depth
D	Depth of tip relief modification
F	Transmitted load
H	Maximum depth of crowning modification
L	Shaft length
N_h	Number of holes
P_0	Maximum pressure
R_b	Base radius
T	Output torque
Z	Number of teeth

Abbreviations

CPU	Central processing unit
DoF	Degree of freedom
FE	Finite element
NVH	Noise, vibration and harshness
PPTE	Peak to peak transmission error
STE	Static transmission error

In general, a preliminary analysis uncoupled from the teeth contact computes the global deformation leading to the shafts misalignment as an input for the STE computation. In fact, it is added to the micro-geometry deviations resulting from tooth profile corrections and manufacturing errors. Notice that these micro-geometry deviations are of the same order of magnitude as tooth and wheel body deformations. Solving the mesh contact force distribution along the contact line is thus nonlinear with the transmitted load.

Another important element for the vibroacoustic behaviour of a gear system is the internal parametric excitation source generated by the meshing stiffness fluctuation. Indeed, the peak-to-peak amplitude of its periodic variation at

the meshing frequency is large. It can reach 65% of its mean value for spur gears, and 40% for helical gears. This internal excitation is deduced from the STE computation as it consists on the slope of the function of the transmitted force versus the STE. This characteristic results from a linear approximation of the transmitted mesh force function. The mesh stiffness is thus expressed as:

$$k(\theta_1) = \frac{\partial F}{\partial \delta(\theta_1)} \tag{2}$$

In classical approaches [5, 19, 30, 49], the contact problem is solved off-line of the finite element analysis including the gear transmission. The contact lines are assumed to be located in the theoretical action plane and the gear static equilibrium is then modelled by separating the gear compliance and the local contact equations along the contact lines [66, 1, 4, 37]. Thus, the gear tooth compliance is preliminarily computed by a finite element analysis or by some alternative analytical tooth bending models using for example Ritz-Galerkin interpolation [14]. Generally, the nonlinear hertzian-like deformation is independently introduced either with an exact or approximate formulation. Furthermore, the potential contact lines located on the theoretical action plane are discretized in small segments where constant punctual forces are applied. Considering the driving angle θ_1, a symmetric semi-positive compliance matrix $\mathbf{H}(\theta_1)$ is introduced for representing the relation between force and displacement at each discretized segment. An initial gap vector, here referred to as $\mathbf{e}(\theta_1)$, describing the initial distance between the teeth on each segment is introduced in order to take into account the tooth flank modifications and manufacturing errors. The misalignment between shafts and the deviation between teeth, induced by the global deformation of the entire transmission, are introduced at this stage. As the static transmission error, noted $\delta(\theta_1)$, fluctuates with the driving angle θ_1 for a given transmitted normal load F, input data (matrix $\mathbf{H}(\theta_1)$, vector $\mathbf{e}(\theta_1)$) are iterated for successive position θ_1, most of the time along a meshing period, involving kinematic analysis of the meshing process. For each position θ_1, the matrix equation representing the mesh contact conditions can be formulated as the following problem:

$$\begin{cases} \mathbf{H}(\theta_1).\mathbf{p}(\theta_1) = \delta(\theta_1).\mathbf{1} - \mathbf{e}(\theta_1) \\ \mathbf{1}^T.\mathbf{p}(\theta_1) = F \end{cases} \tag{3}$$

under the following constraints:

$$\begin{cases} -\sum_j H_j(\theta_1) p_j(\theta_1) + \delta(\theta_1) \geq e_j(\theta_1) \\ p_j \geq 0 \end{cases} \tag{4}$$

In this equation under constraints, the unity column vector $\mathbf{1}$ has all its components equal to 1, the column vector $\mathbf{p}$ is the unknown distributed load to be solved and the scalar function $\delta(\theta_1)$ represents the unknown STE, also to be solved. Different algorithms can be used to obtain the solution ($\mathbf{p}(\theta_1)$, and $\delta(\theta_1)$), the most popular one is based on a modified simplex method [12]. The mesh stiffness is computed by a numerical derivation of the transmitted load F relative to the STE. These classical approaches are similar to the approach used in the software LDP [19] and it is well adapted for cylindrical gears with parallel shafts but are more complex to implement in the case of other geometries as, for example, spiral bevel gears.

Alternatively, Vijayakar [54] combines Finite Element and surface integral methods for solving the analytical contact and the FE solution at surfaces. The finite element model predicts the deformation far away from the contact area but in the contact zone a surface integral form of Boussinesq solution is used to estimate the relative displacement of body points. Then, a "matching interface" is used to combine the finite element solution and the surface integral solution. However, the approach introduced by Vijayakar predicts the size of the contact area assuming an elliptic area as claimed by Hertz theory and this is usually not the case due to the variation of the curvatures at the contact surfaces.

Other authors [9, 10, 11, 42, 62, 63] compute the gear mesh stiffness by using the potential energy method. This method takes into account the bending energy, axial compressive energy, shear energy and hertzian energy. The gear tooth is modelled as a non-uniform cantilever beam and this affects the accuracy of the stiffness estimation. Mark *et al.* [27] propose an analytical expression for the transmission error and the mesh stiffness of helical gears. The expression contains two contributions which are the elastic tooth deformation including the tooth geometric modifications, and the mean deviation of the deformed tooth. Bruyere *et al.* [3] present an analytical approach to describe the transmission error including profile relief and lead crown. The approach allows a fast minimization of the transmission error in narrow-faced helical gears. However, analytical description of the transmission error is based on limited assumptions

and parameters which must be identified. Most of the time, flexible parts of the system are omitted. Analytical methods are thus less accurate than FE-based methods.

After selecting one of the different strategies presented above, the static transmission error and the time varying mesh stiffness are introduced as an internal excitation in order to compute the gear dynamic response [18, 55, 34, 33]. An accurate prediction of the STE and the mesh stiffness are thus essential to compute precisely the dynamic response.

We can also point out that mechanical transmission design in aeronautics and automotive industry is ruled by a search of weight reduction and it often leads to wheel bodies with a thin rim or holes. Usually, a torsional stiffness to model the gear body flexibility is added but it cannot take into account possible twist of the tooth flank in the plane of action.

In this context, the approach considered here is to directly perform a flexible multibody finite element (FE) analysis of the gear pair, in order to evaluate the static transmission error taking into account the nonlinear behaviour induced by the contact between gear teeth. Different strategies to solve the meshing teeth contact through the ANSYS Mechanical ® solver are considered. Considering a flexible FE analysis to model and simulate gears is now achievable thanks to an increase in computer resources. The objectives of the proposed methodology are thus:

- to use a FE-based contact without assumption on the contact lines positions and orientations.
- To define the micro-geometry deviations directly on the 3D gear geometry.
- To simultaneously compute the static transmission error, the root stress and the hertzian shear stress in the contact area.
- To propose a multibody description to take into account the flexibility of the main part of the gear transmission.
- To evaluate a strategy to reduce the computational time compared with the Guyan condensation.

The paper is structured as follows: section 2 describes the FE-based contact formulation used through ANSYS Mechanical ® solver and discusses the use of an augmented lagrangian formalism with a surface-to-surface contact detection. The flexible multibody modelling is introduced in section 3. Then, the multibody strategy is assessed, by comparing the results obtained for a spur gear pair with those from a classical approach and extended to more complex gears: helical gears, spur gear with holed gear blanks, spur gear with flexible shafts and thin rim wheel.

2. FE-based contact through ANSYS Mechanical ® solver

Solving non-linear problems by finite element analysis remains a challenge due to the contact and the nonsmooth mechanics induced by possible contact losses [61, 59, 60, 58]. The contact formulation needs an accurate contact detection algorithm and an appropriate time integration scheme to deal with a large stiffness variation during the contact treatment. Thus, two particular conflicts have to be addressed for describing properly a FE-based contact, corresponding to the increased difficulty in the implementation compared with a classical FE analysis and the large number of degrees of freedom involved associated with the refinement of the mesh needed in the contact zone.

2.1. Contact element definition

In a general contact analysis, the size and form of the contact area is not known in advance and detecting accurately bodies' interaction is essential for an efficient contact analysis. In the case of gears, tooth profile deviations are of the order of a few micrometers which requires a very fine mesh element size of the tooth surface. Thus, the contact detection has to be extremely precise. As shown in Fig. 1, a 8-node contact element intended for 3D geometries and flexible-flexible contact analysis is used. The surface of one body is conventionally taken as a contact surface and the other one as a target surface considering that both surfaces are associated with flexible bodies. In this study, a surface-to-surface contact element is privileged in order to take account of the tooth micro-geometry as opposed to node-to-surface element for which only target nodes are constrained to prevent penetration into the contact surface. Indeed, in this formulation, the contact conditions are introduced so that each target node interacts with a projected point on the contact surface. Consequently, contact conditions involve a single node and it concentrates the force at this node. So, node-to-surface facilitates unintended penetration during the contact detection and it leads to less precise stress and pressure. In contrast, the target surface can penetrate into the contact surface for the surface-to-surface element and this interpenetration tolerance has to be adjusted in regards to the tooth profile modifications. This surface

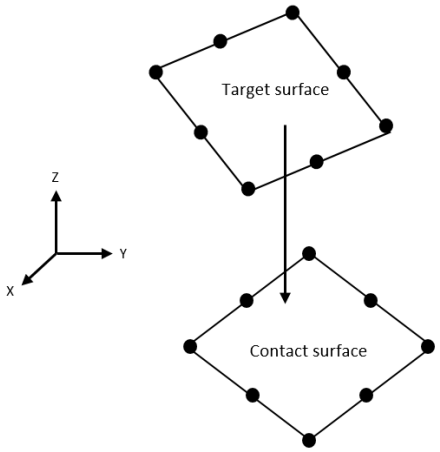

Figure 1: 8 nodes surface-to-surface contact element.

is projected on the contact surface and the contact detection points are the integration points which are either nodal points or gauss points [8]. Contact inequalities are expressed at integration points and gauss points represent sampled discrete points on the surface element. 4 gauss points on the surface contact element are considered. They are integrated on the surface using corresponding weight factors. The node values are then obtained with shape functions using the value of the nearest corresponding gauss points. The interpenetration is handled on the target surface and its integration points along the normal direction [7]. The surface-to-surface element involves more nodes during the contact treatment which has a smooth effect on the stress and the pressure. Indeed, contact forces do not jump when a contact node slide off the edge of a target surface because contact forces are computed even when it is only partially in contact. The surface-to-surface element provides thus a more accurate computation of contact stresses for the contacting elements considered.

2.2. Frictionless contact formulation

Several contact algorithms are associated with the previous contact element. The pure penalty method, augmented lagrangian method and pure lagrange multiplier method are largely used in FE softwares and particularly in the ANSYS Mechanical ® solver. In this paper, we focus on frictionless contact because vibroacoustic phenomena in gear transmission are mainly caused by the fluctuation of the normal contact force at the gear pair [6, 40]. If one is interested in power losses, friction and therefore tangential contact forces, should be considered [23, 53].

Contact formulation can be classified into two categories corresponding to penalty methods and lagrangian methods. The pure penalty method received a larger approval in the literature due to its implementation convenience. It consists in adding a penalty term represented by a nonphysical (or mathematical) contact stiffness but the main drawback is that the amount of penetration between the two surfaces depends on this stiffness [15, 48, 41]. For this reason, the penalty formulation can lead to ill-conditioned problems and inaccurate solutions. The pure lagrangian method uses a lagrange multiplier as an added degree of freedom and this approach enforces zero penetration. It does not require additional stiffness but it needs more iterations to reach contact conditions convergence and therefore it is computationally demanding [35]. This method can also lead to inaccurate solutions because the method overconstrains the model and needs much more iterations to reach the convergence compared with the pure penalty method. Another method named the Augmented Lagrange Multiplier method [45, 25] has been developed to keep the advantages of the two previous contact formulations. The approach is an iterative combination of the penalty method and lagrange multiplier formulation. Compared to the penalty method, the augmented lagrangian method usually leads to better conditioning and is less sensitive to the magnitude of the contact stiffness coefficient. The impenetrability is thus achieved while improving the convergence. The augmented lagrangian formulation is retained to describe the gear contact. To every contact node or gauss point i associated to mesh elements corresponds a gap function d_i measuring the distance between the contact and the target surfaces along the normal direction. F_i is the contact force acting on

the target surface. The nonsmooth mechanics is thus represented by Signorini conditions [58, 59, 60]:

$$\begin{cases} d_i \geq 0 \\ F_i \geq 0 \\ d_i F_i = 0 \end{cases} \qquad \forall i, \tag{5}$$

The constraints $d_i \geq 0$ and $d_i F_i = 0$ represent the impenetrability and complementarity conditions. The contact forces $F_i \geq 0$ are generated only when the gear tooth contact occurs ($d_i = 0$), while the contact forces are zero ($F_i = 0$) when the gear tooth contact is lost ($d_i > 0$). The contact force F_i acting on the target surface is defined by:

$$F_i^j = \kappa d_i^j + \lambda_i^j \tag{6}$$

κ is the mathematical stiffness coefficient, λ_i^j is the iterative lagrange multiplier associated to the contact node i at the iteration j which is updated until d_i^j is sufficiently small (i.e $d_i^j \leq \epsilon$, typically $\epsilon = 10^{-2}$) [25, 45].

3. Problem formulation

3.1. Gear geometry definition

In the study, we focus on spur and helical gears transmitting power between parallel shafts. The tooth geometry definition received a particular attention. As mentioned in the introduction, tooth profile deviation from the theoretical involute tooth profile is of the order of a few micrometers. Therefore an accurate geometry generation is needed. Indeed, the generation is performed using high order Non-Uniform Rational Basis Splines with a high control point number. It is shown in [43, 50] that Non-Uniform Rational Basis Splines lead to better accuracy for contact problems without considering profile deviation.

Here, we introduced two types of tooth deviations from the theoretical involute tooth profile: a longitudinal crowning (see Fig. 2b) and a linear tip relief (see Fig. 2a). They are intentional removal of material from gear tooth flanks. They help reducing dynamic loadings and compensate shafts misalignment and deflections. Longitudinal crowning is generally introduced to maintain the contact at the tooth flank centre and linear tip relief smoothens the meshing transition process.

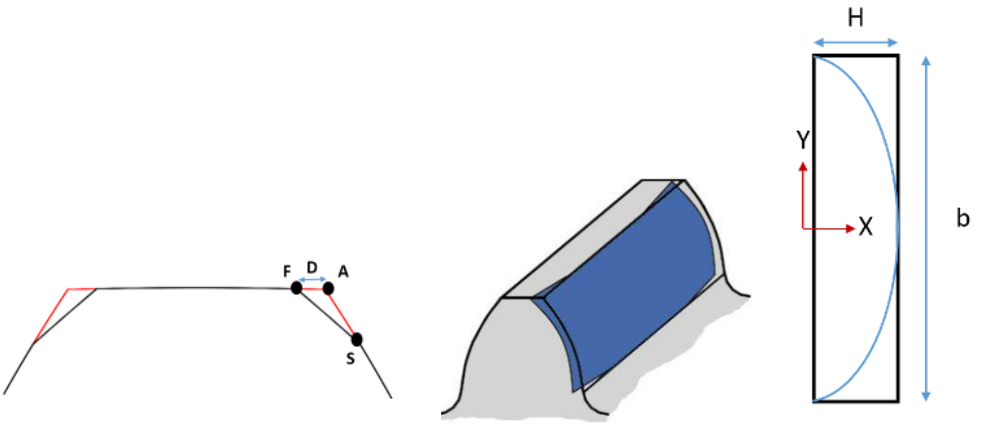

Figure 2: Description of linear tip relief deviation (a) where S is the starting point, D is an amount of profile modification at the tooth tip starting from point A to the point F. Longitudinal crowning modification (b) and parameters description from the top (c). H is the maximum depth of crowning.

3.2. Multibody gear simulation

The problem to solve the gear dynamics is expressed as follow:

$$\mathbf{M}\ddot{\mathbf{x}} + \mathbf{C}\dot{\mathbf{x}} + \mathbf{K}\mathbf{x} + \mathbf{F}_{nl}(\mathbf{x}) = \mathbf{F}_{ext} \tag{7}$$

where $\mathbf{x}$ contains the generalised displacement of each degree-of-freedom and $\mathbf{M}$, $\mathbf{C}$, $\mathbf{K}$ are respectively the mass, damping and stiffness matrix. $\mathbf{F}_{nl}$ is the contact force and $\mathbf{F}_{ext}$ is the vector of external forcing. The approach presented here is focusing on the quasi-static behaviour of the gear pair. Indeed, the dynamic equation (7) is solved for a slow rotation of the driving gear (1 rpm) and the dynamical effects are needed only to improve the convergence during the gap covering.

It is a scientific progress to deal directly with flexible multibody analysis in quasi-static operating conditions for evaluating the transmission error, especially to show complex effects of the gear mesh process. Indeed, the contact treatment phase (contact detection and contact force computation) is solved in real operating conditions. So, specific gear mesh behaviour is brought to light compared to classical methods. The multibody modelling approach aims at providing a generic model that can be used as a reference for meshing settings, contact settings and loading conditions. The proposed methodology intends to accurately identify the gear internal excitation. For this purpose, the procedure, the implementation and the results precision are evaluated. As mentioned in the previous section, a fine mesh is of paramount importance to highlight the influence of the load level but also to take into account the hertzian deformation and the micro-geometry. Knowing that the tooth deformation takes account of tooth deflection and local hertzian-like deformation induced by the contact, the mesh has to be refined accordingly in the contact area. Moreover, a nonlinear analysis must be carried out for various levels of output torque to show the effect of load on the tooth deformation. To achieve the simulation, three steps have to be set up:

- firstly, the gear backlash is covered by a rotation of the driving wheel in order to establish the contact at an initial state.
- Then, while the rotation of the driving wheel is fixed, the output torque is applied on the driven wheel.
- Finally, a rotation of the driving wheel is performed over a period corresponding to the fundamental period of static transmission error (at least one mesh period).

A control node is defined at each gear centre to apply boundary conditions and to measure the time varying input and output gear angles. The static transmission error $\delta(\theta_1)$ is then computed along the line of action and the mesh stiffness $k(\theta_1)$ is approximated by a numerical differentiation of the transmitted load F versus $\delta(\theta_1)$. The discretization of the angular position of the driving wheel has to be finely defined for describing properly the sudden variation of the STE. At least 40 points over one mesh period are needed. In addition, to avoid numerical errors, the differentiation of the mesh stiffness is achieved by taking a centred differentiation step equal to 15% of the load and the STE.

4. Results and discussion

4.1. Preliminary validations

This section is a preliminary analysis of the proposed methodology in order to optimally compute the static transmission error. Firstly, the influence of the mesh on the STE is evaluated. Then, the time cost is reduced through an optimal selection of computer resources. The pre-processing and post-processing phase of the multibody approach and the classical approach are of similar computation time. So, preliminary validations are established on the resolution procedure over two mesh periods for a given output torque. The value of the parameter κ defined in the eq. (6) is set to 10^{17}. This value provides a good compromise between the convergence and the penetration which is thus less than a micrometer.

4.1.1. Mesh convergence

To propose an efficient multibody simulation, a convergence study on the FE mesh along the tooth was carried out. We consider three mesh cases corresponding to 50, 70 and 100 hexa-linear elements along the involute profile. It corresponds to a mesh element size of 70 μm, 50 μm and 38 μm, respectively. For these three cases, an equal inflation of 30 layers for the bulk and up to 30 elements along the tooth width (with 0.6 mm length) are introduced.

The inflation measures 900 μm with a depth of each layer equal to 30 μm. At the pitch contact point, an estimated shear stress [20] beneath the surface at 900 μm is less than 15% of the maximum value. Additionally, for the different mesh considered, the estimated contact width predicts 3 to 6 elements along this width. This dense mesh size makes us confident to capture edge effects and hertzian-like deformation. Validations will be established by comparing with analytical formula of Hertz theory.
At this stage, our objective is to evaluate and capture the effect of the micro-geometry. So, firstly, we compute the unloaded transmission error for the three mesh cases. The procedure is applied for validation on a spur gear pair considering the following gear characteristics (Table 1). This reverse gear pair is designed for a nominal torque $T = 100\,\mathrm{N\,m}$.

Name	Designation	Gear 1	Gear 2	Unit
Module	m_n	2		mm
Number of teeth	Z	50	50	-
Pressure angle	α	20		deg
Contact ratio	ϵ_α	1.512		-
Base radius	r_b	46.985	46.985	mm
Profile shift coefficient	x	0	0	-
Addendum	h_a	2	2	mm
Dedendum	h_f	2.5	2.5	mm
Face width	b_f	20	20	mm
Center distance	a'	100.5		mm
Tip relief modification				
Starting radius	r_S	50.26	50.26	mm
Depth	D	5	5	μm
Longitudinal crowning modification				
Maximum depth	H	0	0	μm

Table 1: Characteristics of the spur gear

The mesh generation with about 700000 nodes and about 2 million degrees-of-freedom is presented in Fig. 3 with a close-up (see Fig. 3b) in the teeth region. The nonlinear quasi-static analysis is carried out for a low output torque

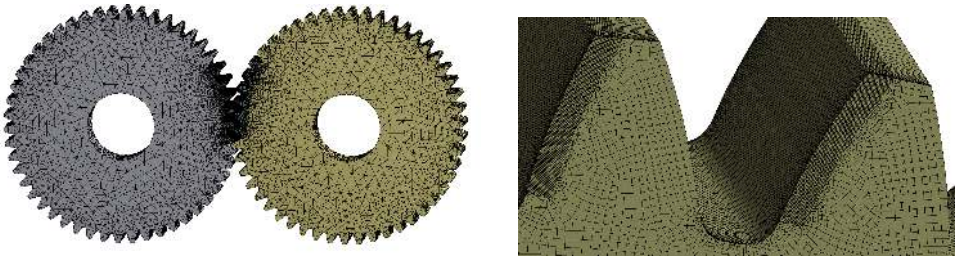

(a) (b)

Figure 3: (a) the spur gear mesh with hexa-linear element at the tooth and tetra element elsewhere (b) close-up of the tooth mesh with 100 hexa-linear element and an inflation.

$T = 0.5\,\mathrm{N\,m}$. The associated unloaded STE is presented in Fig. 4 for different levels of detail of the tooth mesh. The shape of the curves follows the long tip relief of 5 μm only for an element size lower than 50 μm. The comparison of the unloaded transmission error exhibits the importance of dealing with a specific mesh. With a precision lower than 1 μm, 70 divisions in the involute profile is a necessary condition. We will verify that this condition is sufficient to take into account transmission error under load including global deformation and hertzian-like deformation.

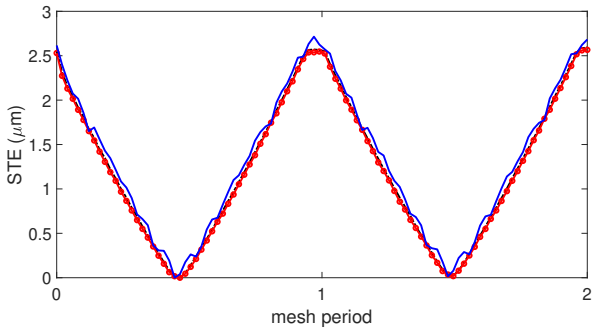

Figure 4: Unloaded transmission error for coarse mesh (50 divisions, —), intermediate mesh (70 divisions, •) and fine mesh (100 divisions, - -).

4.1.2. Time cost

The Guyan condensation [16] is largely used in solid mechanics for solving the static analysis of contacting structures. The approach provides an exact solution of nonlinear problems while improving the time cost compared with a direct solving. The idea is to consider two sets of degrees of freedom (DOF), one for active u_A (contact nodes here) and another complementary u_C. The DOF separation allows the identification of a linear relationship between the two sets of DOF:

$$\mathbf{u}_C = -\mathbf{K}_{CC}^{-1}\mathbf{K}_{CA}\,\mathbf{u}_A \tag{8}$$

where the finite element stiffness K is split into four blocks:

$$\begin{bmatrix} \mathbf{K}_{AA} & \mathbf{K}_{AC} \\ \mathbf{K}_{CA} & \mathbf{K}_{CC} \end{bmatrix} \tag{9}$$

Considering our gear model, about 6000 contact nodes are possibly involved during the contact treatment. A refinement of the mesh at the contact interface leads to full matrices after the condensation on the nonlinear degrees of freedom. So, the matrix operation shown in the equation (8) becomes computationally demanding. To overcome this difficulty, we investigate a direct resolution of the full system using domain decomposition.

Domain decomposition is a parallel computation technique widely used in computational mechanics [22, 31, 64]. It consists in the division of the whole domain in several partitions. The mechanical problem is solved independently on each partition and an update of the boundaries enables communication between the partitions. Herein, we apply a domain decomposition on a cluster using CPU resources (1 computer node = 16 cores, 2.6 GHz and 64 GB RAM) in order to achieve the flexible multibody simulation. A parametric study on the case presented in Table 2 is conducted by increasing the CPU resources from 16 cores (1 computer node) to 96 (6 computer nodes). The simulations are benchmarked against the Guyan method.

Simulations	Time cost (s)	Time reduction (%)	Number of cores
REF (Guyan)	144000	-	-
1	53224	63%	16
2	18303	87%	32
3	15286	89%	64
4	19226	86%	96

Table 2: Parametric study on spur gear to reduce the time cost

Table 2 displays the time cost for simulations over two mesh periods. Figures in Table 2 show that 64 cores is the optimal choice for solving the nonlinear analysis. Constantly increasing the domain discretization is not leading to a proportional constant time reduction. Indeed, for 96 cores the time reduction (86%) is less than for 64 cores. This is induced by the large number of information transfers needed to communicate with each partition. The multibody analysis is thus performed in the following sections by solving the full nonlinear system using 64 cores.

4.2. Numerical comparison with a classical approach

The objective of this section is to evaluate the main differences between the proposed multibody methodology and the classical approach described in the introduction and based on the eq. (3) and (4). This approach is implemented in a software named TERRA [30, 37] developed by the joint laboratory "gear dynamics laboratory LADAGE". For this code, the compliance matrix $H(\theta)$ is computed with an analytical thick plate model to evaluate the tooth strain energy and a Ritz-Galerkin approximation to evaluate the tooth deflection [14]. The assessment is made in terms of static transmission error and meshing stiffness fluctuations. The gear transmission presented in Table 1 is retained for the comparison. The study is performed for various output torques in order to obtain relevant comparative results. Then, the potential effects on the dynamic behaviour are discussed.

4.2.1. Static transmission error

Several nonlinear analyses are carried out for different output torques and a map of the static transmission error is built. Fig. 5a and Fig. 5b are respectively the maps of the STE using the multibody method and the classical approach. The gear mesh procedure is properly handled by the multibody approach and the periodicity of the STE is well represented. Fig. 5a and Fig. 5b show a good match between the transmission curves for an output torque from 0.5 N m to 50 N m. Indeed, the tip relief of 5μm is clearly identified by both approaches. However, for a torque level up to 50 N m, the classical approach underestimates the mean values of the STE while the STE shapes have a smoother variation using the multibody method. In fact, the transition from one tooth pair to another is progressively handled as shown in Fig. 6. Indeed, in Fig. 5b, a sudden variation of the STE is visible for a torque equal to 50 N m which can be explained by a brutal transition of the number of teeth pair involved during the contact treatment. This phenomenon is amplified as the torque is increased. In the classical approach, the contact lines positions and orientations and therefore the contact ratio of the gear pair (expressed as $\epsilon_\alpha = g_\alpha/p_b$ while g_α is the length of path of contact and p_b is the base pitch) are determined a priori. This explains the brutal variation of the STE.

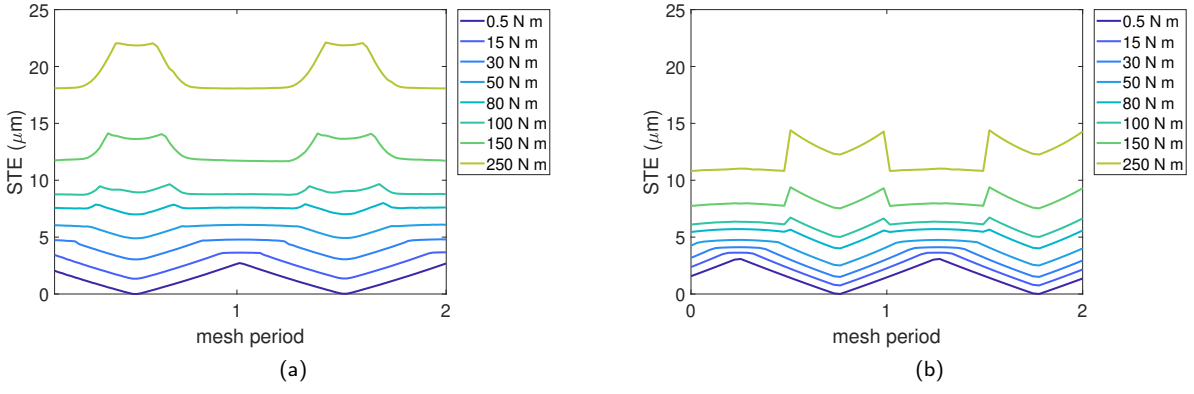

Figure 5: The static transmission error for different torque levels $T = [0.5, 15, 30, 50, 80, 100, 150, 250]$ N m and over two mesh periods. Numerical results through ANSYS Mechanical ® solver (a) and the classical method (b).

Moreover, the map brings to light the nonlinear variation of the STE in regards to the load. The peak to peak transmission error (PPTE) is measured from the STE map for the proposed approach (Fig. 5a) and the classical approach (Fig. 5b) in order to highlight the relation between load and deformation. The variations of the PPTE presented in Fig. 7 allow an estimation of an optimal torque. Indeed, the PPTE amplitude of the classical approach decreases until a minimum value for an output torque close to $T = 70$ N m, whereas for the multibody approach the minimum value is reached for an output torque $T = 100$ N m. The optimal torque ranges for the classical approach and the multibody approach are respectively $[80, 150]$ N m and $[60, 110]$ N m. Differences in the estimation of the optimal torque and the mean value of the STE can be explained on the one hand by the method retained in the classical strategy for the computation of the compliance matrix $H(\theta)$ and on the other hand by the number of teeth detected during the contact treatment as mentioned above. These differences can lead to an imprecise micro-geometry optimization when using standard methods.

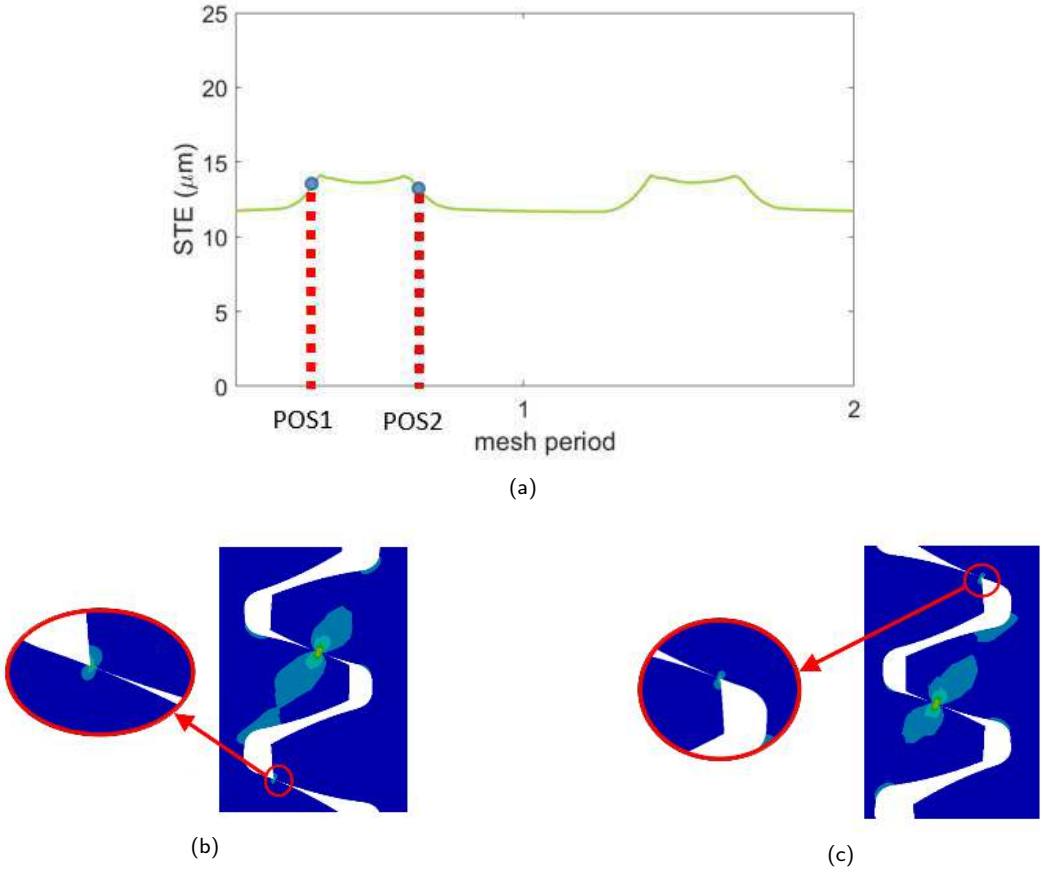

Figure 6: STE for 150 N m with two contact positions named POS1 and POS2 (a). A close-up at the contact POS1 (b) and POS2 (c).

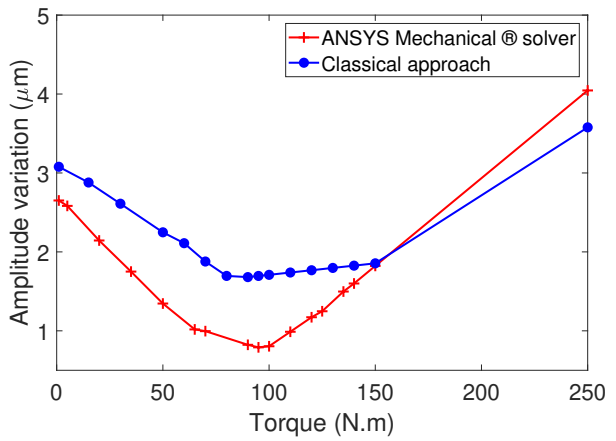

Figure 7: Comparison of the different peak to peak transmission error (a): —Classical approach, and —ANSYS Mechanical ® solver.

4.2.2. Mesh stiffness

The different mesh stiffness are evaluated for the output torques $T = [0.5, 15, 30, 50, 80, 100, 150, 250]$ N m over two mesh periods. The mean value and the fluctuations of the mesh stiffness of the proposed methodology and the classical approach are both governed by the output torque as shown in Fig. 8. It appears three ranges of variation corresponding to: low torque $[15, 50]$ N m, medium torque $[50, 100]$ N m and high torque $[100, 250]$ N m.

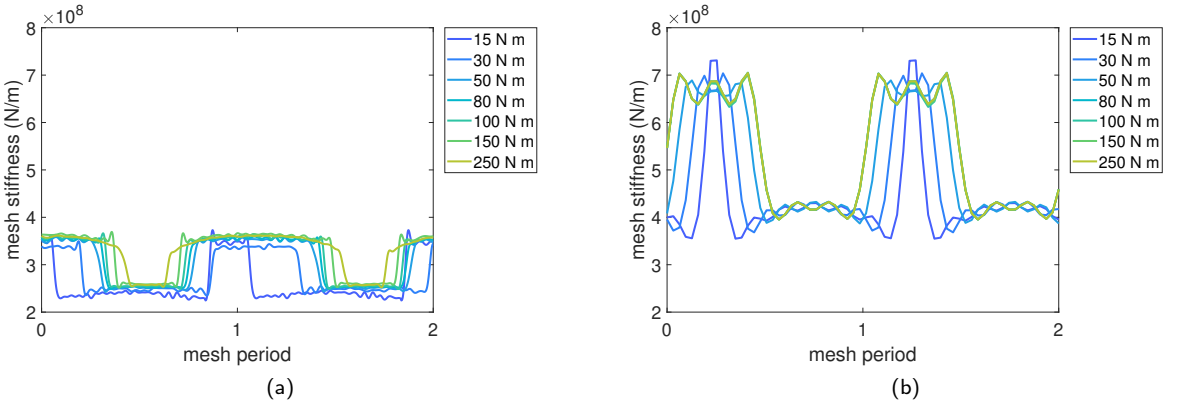

Figure 8: Mesh stiffness for different torque levels $T = [15, 30, 50, 80, 100, 150, 250]$ N m: (a) ANSYS Mechanical ® solver and (b) classical approach.

The mean values of the different mesh stiffness computed through the multibody approach are half of the ones obtained with the classical approach. The critical modes which are the modes for which the strain energy contribution at the mesh is maximum are governed by the mean value of the mesh stiffness. The critical frequencies of the system are thus re-ordered. This change affects the critical operating speeds of the system. In addition to this, as shown in Fig. 8, the fluctuations of the different mesh stiffness are also half of the ones obtained for the multibody method compared with the classical approach. Obviously, the mean values of the different mesh stiffness are different since the flexibility of the gear body is not taken into account in the classical approach. However, differences are also related to the fact that the classical approach does not allow a good description of the contact treatment between the gear teeth and also the hertzian-like deformation. In contrast, the proposed approach based on a multibody description and a surface-to-surface contact element allows an accurate contact treatment since no assumption are made on the contact point locations and the global and local deformation are taken into account. The large variation observed modifies parametric phenomena and the amplitude of resonance of the dynamic response [51].

4.2.3. Normal contact characteristics of mating gear teeth

It is of paramount importance to evaluate the normal characteristics of mating gear teeth. The local contact behaviour is often modelled with Hertz theory [20]. It is an efficient way to approximate local deformations and to predict contact areas. Herein, the mutlibody approach through ANSYS Mechanical ® solver provides stress, contact pressure and contact area with no assumption of the contact curvature. The objective of this section is thus to compare the physical quantities determined and quantified with the multibody approach and those obtained with analytical formula of Hertz theory for two infinite cylinders under load [20].

The cylindrical Hertzian contact stress theory for two infinite cylinders under load is based on the following assumptions:

- the surfaces are continuous and non-conforming.
- Each interacting body is considered as an elastic half-space with small strains.
- It is a frictionless contact.
- The contact areas are small compared to the size of the radii of curvature of surfaces.

The curvature radii at the contact point of two cylinders are represented in gears by the tangential segments of the base radii connected to the contact point. For a contact point close to the pitch radius, the contact width h, the contact depth z_0, the maximum pressure P_0 and the maximum shear stress τ as described in Fig. 9 are compared with the multibody approach (see Table 3). The contact width is accurately approximated with the multibody approach. Indeed, as shown in Table 3, the approach generates 229μm of contact width and 204μm is accounted for Hertz theory. Additionally, the contact analysis converged in terms of maximum pressure and maximum shear stress as depicted in Table 3 where only 20 MPa of differences with Hertz are measured. The results obtained with the proposed approach are thus in good agreement with the those acquired by Hertz theory. In contrast, these physical quantities can't be retrieved directly with a classical approach. It requires additional analyses.

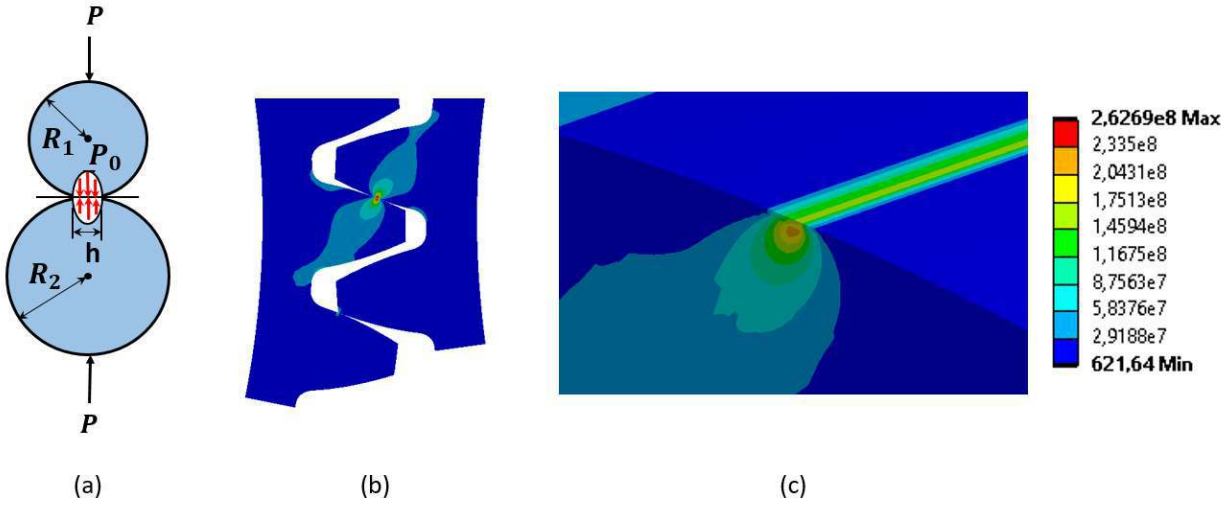

Figure 9: (a) Description of the cylindrical contact stress claimed by Hertz theory, (b) shear stress for a torque of $T = 100\,\mathrm{N\,m}$ and (c) a close-up of the shear stress in Pa at the middle of the tooth width is depicted.

Physical quantities	Analytical results of Hertz theory	Proposed approach	Difference (%)	Unit
h	204	229	12	μm
P_0	663	643	3	MPa
τ	199	221	11	MPa
z_0	79.5	98.3	23	μm

Table 3: Comparative study on spur gear with Hertz theory

4.3. Capability of the multibody method to detect specific phenomena

The study carried out in this section, applies the proposed multibody approach to several gear transmissions in order to show the large possibility of the method and to bring to light some phenomena. The gear pairs are classified in three test cases. The first case compares a gear pair with a longitudinal crowning to a gear pair without. Then, the effect of thin rim and flexible shaft on spur gear is evaluated. Finally, modulations in time and frequency domains of a spur gear with holed gear blanks are identified. These phenomena are not properly taken into account with classical approaches. To identify these specific effects, the fluctuations of the STE for an output torque of $T = 115\,\mathrm{N\,m}$ are thus computed, described and discussed.

4.3.1. Effect of crowning

The reverse helical gear pair with longitudinal crowning, also defined for a 100 N m nominal torque, is described in Table 4 and its geometry is reported in Fig. 10. This gear pair is compared with the same helical gear pair without

crowning modification. A control node is defined at each gear centre to apply boundary conditions. Translations of the gear pair are prevented for each control node. Control nodes of the driving and the driven gears are used to apply the driving rotation θ_1 and the output torque T. Fig. 11 displays the STE fluctuations of the helical gear pairs. The longitudinal crowning modifies the shape of the STE and it appears a larger curvature as shown in Fig. 11b. The peak to peak amplitude increases significantly until it reaches 2μm compared with the standard helical gear pair (see Fig. 11a). These effects on the STE are explained by the fact that the contact force is localized at the tooth flank center.

Name	Designation	Gear 1	Gear 2	Unit
Module	m_n	2		mm
Number of teeth	Z	50	50	-
Pressure angle	α	20		deg
Helix angle	β	15		deg
Total contact ratio	ϵ_t	2.275		-
Base radius	r_b	48.439	48.439	mm
Profile shift coefficient	x	0	0	-
Addendum	h_a	2	2	mm
Dedendum	h_f	2.5	2.5	mm
Face width	b	20	20	mm
Center distance	a'	104		mm
Tip relief modification				
Starting radius	r_S	52.024	52.024	mm
Depth	D	5	5	μm
Longitudinal crowning modification				
Maximum depth	H	10	10	μm

Table 4: Gear characteristics of the helical gear pairs.

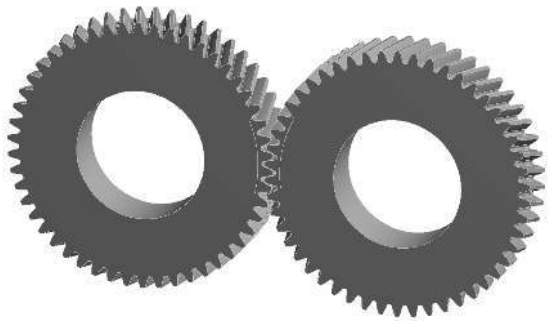

Figure 10: Helical gear pair.

4.3.2. Effect of thin rim and flexible shafts

This section analyzes the influence of a thin rim wheel and flexible shafts on the STE fluctuations. The thin rim is located in the midplane of the gears but the gears are not at the center of the shafts in order to accentuate possible rotation of the tooth flank in the plane of action. The Table 5 described in detail the micro and macro geometry and the gear pair is depicted in Fig 12. A control node is defined at each face centre of the driving and driven shafts to apply boundary conditions and translations of shafts are prevented. Control nodes of the driving and the driven shafts are used to apply the driving rotation θ_1 and the output torque T. The STE fluctuations are compared with those presented in Fig. 7, for which a spur gear without thin rim and shafts is considered. The shape of the curve is modified and the

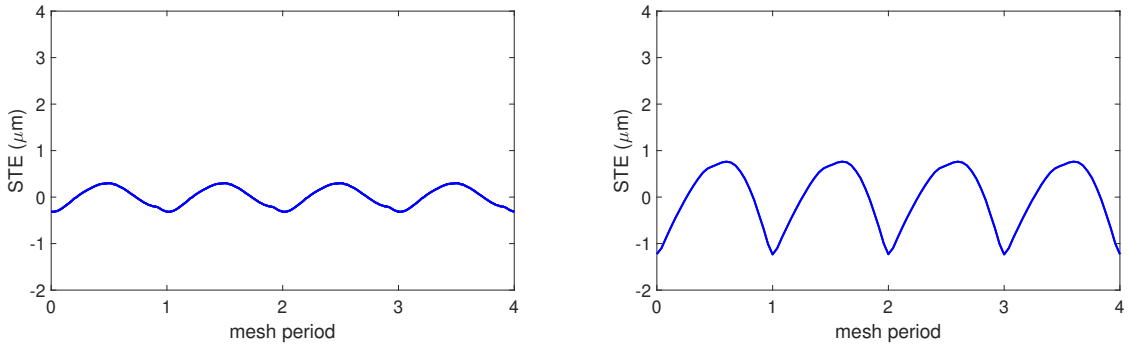

Figure 11: Fluctuation of the static transmission error over 4 mesh periods for an output torque $T = 115\,\mathrm{N\,m}$: (a) helical gear without longitudinal crowning, (b) helical gear with longitudinal crowning of 10μm.

peak to peak amplitude is increased from 1 μm (see Fig. 7) to 4 μm (see Fig. 13).

Name	Designation	Gear 1	Gear 2	Unit
Module	m_n	2		mm
Number of teeth	Z	50	50	-
Pressure angle	α	20		deg
Contact ratio	ϵ_α	1.512		-
Base radius	r_b	46.985	46.985	mm
Profile shift coefficient	x	0	0	-
Addendum	h_a	2	2	mm
Dedendum	h_f	2.5	2.5	mm
Face width	b	20	20	mm
Center distance	a'	100.5		mm
Tip relief modification				
Starting radius	r_S	50.26	50.26	mm
Depth	D	5	5	μm
Rim wheel dimension				
Rim width	b_w	8	8	mm
Shaft dimension				
Shaft length	L	300	300	mm

Table 5: Gear characteristics of the spur gear with thin and flexible shafts.

Moreover, the deformation of the shaft induces a misalignment as shown in Fig. 14a. Indeed, the contact pressure is partially distributed on the tooth flank when the gear teeth are in contact. This particularity is accounted in-line with the multibody approach which is not the case for a classical approach for which the contact is based on the theoretical contact lines. All couplings of the gear transmission are taken into account during the STE computation and this affects significantly the contact pressure distribution and the STE fluctuations. Off-line of action contact has been identified by Singh *et al.* in [46]. However, the proposed approach based on FE contact allows an accurate description of the contact condition without additional geometrical consideration and taking into account micro-geometry deviations.

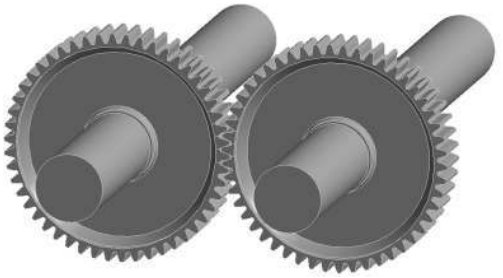

Figure 12: Spur gears with thin rim and flexible shafts

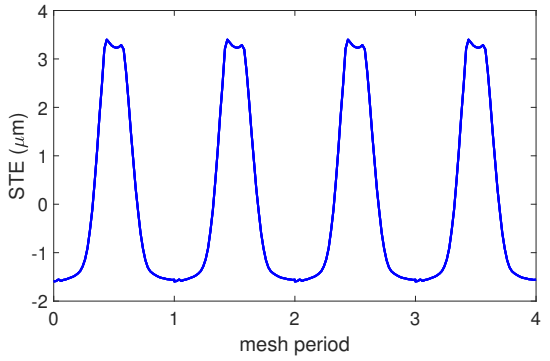

Figure 13: Fluctuation of the static transmission error over 4 mesh periods for an output torque of 115 N m.

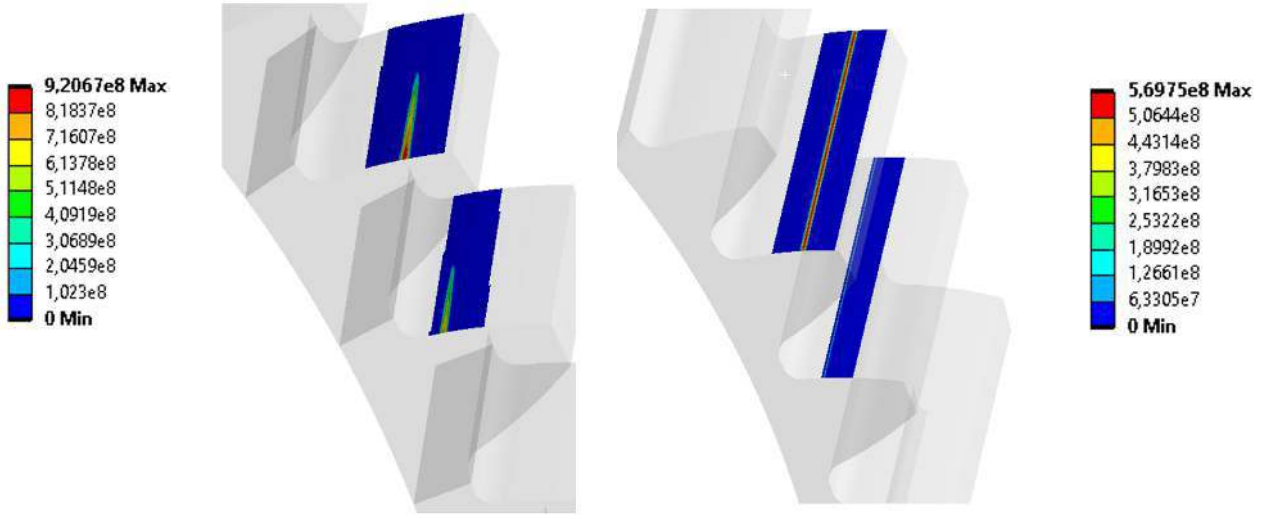

(a) (b)

Figure 14: Contact pressure distribution on the mating teeth in Pa: (a) spur gear with thin rim and flexible shafts, (b) standard spur gear.

4.3.3. Effect of gear body with holes

This part investigates the influences of holed gear blanks on the STE fluctuations. We consider a spur gear with 8 holes on each gear bodies as shown in Fig. 15. A control node is defined at each gear centre to apply boundary conditions. Translations of the gear pair are prevented for each control node. Control nodes of the driving and the driven gears are used to apply the driving rotation θ_1 and the output torque T. Fig. 16 displays STE fluctuations and the frequency spectrum. Holes in gear blanks are responsible for additional harmonic components, especially at low frequency. Indeed, a harmonic corresponding to the number of holes is created and this amplitude exceeds the mesh harmonic (see Fig. 16b).

The harmonic content show also the existence of sidebands. Considering H_Z and H_{N_H} which are respectively the mesh harmonic and the harmonic of holes, we can identify sidebands as $H_{sb} = H_Z \pm H_{N_H}$. For example on the Fig. 16b we see the harmonics H_{42},H_{50} and H_{58}

So, changes in gear blank topology increase the harmonic content of the STE. This phenomena is not properly handled within the state-of-the-art strategies for which the contact is established at the theoretical contact lines.

Name	Designation	Gear 1	Gear 2	Unit
Module	m_n	2		mm
Number of teeth	Z	50	50	-
Pressure angle	α	20		deg
Contact ratio	ϵ_α	1.512		-
Base radius	r_b	46.985	46.985	mm
Profile shift coefficient	x	0	0	-
Addendum	h_a	2	2	mm
Dedendum	h_f	2.5	2.5	mm
Face width	b_f	20	20	mm
Center distance	a'	100.5		mm
Tip relief modification				
Starting radius	r_S	50.26	50.26	mm
Depth	D	5	5	μm
Lightweighting				
Number of holes	N_H	8	8	-
Radius of holes	r_H	20	20	mm

Table 6: Gear characteristics of the spur gear with holed gear blanks.

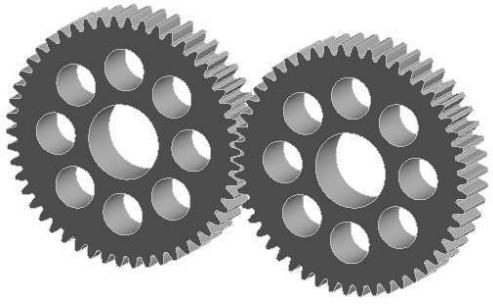

Figure 15: Spur gear with holed gear blanks.

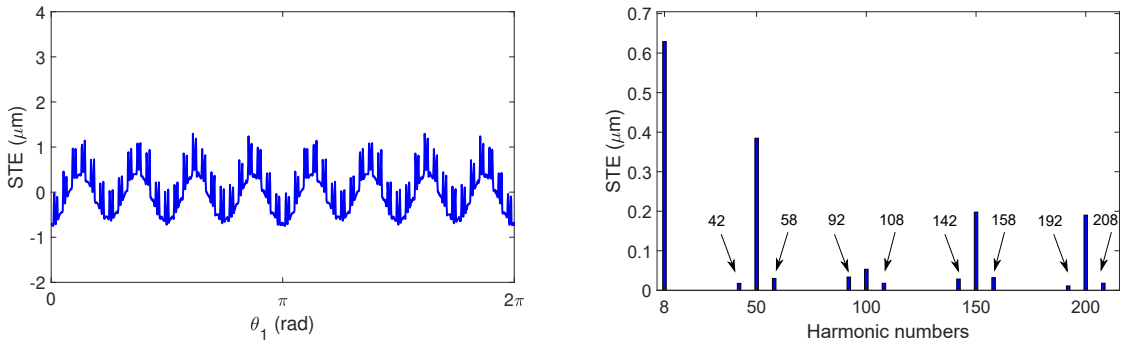

(a) (b)

Figure 16: Fluctuation of the static transmission error of the gear pair with holes (a) and frequency spectrum (b) for an output torque $T = 115$ N m.

5. Conclusion

A flexible multibody approach through ANSYS Mechanical ® solver is proposed to deal with gear mesh contact. The complete nonlinear problem is solved numerically by performing dynamic analysis at low rotating speed (1 rpm). The main contributions of the proposed approach are:

- to consider a FE-based contact without assumptions about the contact lines positions and orientations.
- To detect with precision the micro-geometry using high order non-uniform rational basis splines and a fine mesh.
- To capture the local hertzian-like deformation of the loaded tooth during the meshing process.
- To recover instantaneously static transmission error, mesh stiffness, root stress and normal contact characteristics of the tooth.
- To take into account the flexibility of many mechanical components of a gear transmission.
- To propose a efficient strategy based on domain decomposition for solving efficiently the multibody contact problem.

It was demonstrated that the investigated method can simulate large sort of gears. Besides, quasi-static numerical results of spur and helical gears showed differences in terms of static transmission and mesh stiffness compared with a classical approach. Indeed, a smoother transition from one tooth to another is identified. The mean values and the fluctuations of the different mesh stiffness are half of those obtained with the classical approach. These results have significant influences on the vibroacoustic behaviour of gears. The differences are mainly due to the multibody description and the contact element. Indeed, the multibody description allows a good representation of the global deformation (deflection of the gear pair) and the local deformation (hertzian-like deformation). Moreover, The contact element is based on no assumptions about the contact lines positions and orientations and it provides a more accurate computation of the contact forces since no jump occurred when a contact node leaves the edge of the target surface.

Furthermore, the proposed methodology can include micro-geometry deviations, additional flexible mechanical components and specific design of the gear body. It thus allows to exhibit complex behaviours. For instance, crowning modification increases the STE fluctuations. Flexible shafts and thin rim provide misalignment, and therefore partial contact pressure distribution at the tooth flank. Holes in the gear blanks add non negligible harmonics components in the STE. However, the approach needs high performance computing (CPU resources) to be applied. The proposed methodology becomes essential to analyze a large variety of gears for which contact lines are difficult to pre-determine due to the geometrical complexity of the tooth surfaces (bevel gears, spiral gear, hypoid gears, worm gears etc.).

Acknowledgements

The authors would like to thanks ANSYS and the ANRT (French National Association for Research and Technology) for their support via a CIFRE grant. This work was performed within the framework of the LabCom LADAGE (LAboratoire de Dynamique des engrenAGEs), created by the LTDS and the Vibratec Company and operated by the French National Research Agency (ANR-14-LAB6- 0003). It was also performed within the framework of the LABEX CeLyA (ANR-10-LABX-0060) of Université de Lyon, within the program « Investissements d'Avenir » (ANR-16-IDEX-0005) operated by the French National Research Agency (ANR). Special thanks go to A.Mélot from LTDS for the critical reading of the manuscript.

Conflict of interest

The authors declare that they have no conflict of interest.

References

[1] Andersson, A., Vedmar, L., 2003. A dynamic model to determine vibrations in involute helical gears. Journal of Sound and Vibration 260, 195–212.

[2] Benatar, M., Handschuh, M., Kahraman, A., Talbo, D., 2019. Static and dynamic transmission error measurements of helical gear pairs with various tooth modifications. journal of mechanical design, 141(10) .

[3] Bruyere, J., Velex, P., Guilbert, B., Houser, D., 2019. An analytical study on the combination of profile relief and lead crown minimizing transmission error in narrow-faced helical gears. Mechanism and machine theory, 136, 224-243 .

[4] Cai, Y., 1995. Simulation on the Rotational Vibration of Helical Gears in Consideration of the Tooth Separation Phenomenon (A New Stiffness Function of Helical Involute Tooth Pair). Journal of Mechanical Design 117, 460–469. American Society of Mechanical Engineers Digital Collection.

[5] Carbonelli, A., Perret-Liaudet, J., Rigaud, E., Le Bot, A., 2011. Particle Swarm Optimization as an Efficient Computational Method in order to Minimize Vibrations of Multimesh Gears Transmission. Advances in Acoustics and Vibration, 2011 .

[6] Carbonelli, A., Rigaud, E., Perret-Liaudet, J., 2016. Vibro-Acoustic Analysis of Geared Systems—Predicting and Controlling the Whining Noise. In Automotive NVH Technology (pp. 63-79) .

[7] Cescotto, S., Charlier, R., 1993. Frictional contact finite elements based on mixed variational principles. International Journal for Numerical Methods in Engineering 36(10), 1681–1701.

[8] Cescotto, S., Zhu, Y.Y., 1994. Large strain dynamic analysis using solid and contact finite elements based on a mixed formulation; application to metal forming. Journal of Materials Processing Technology 45(1-4), 657–663.

[9] Chen, Z., Shao, Y., 2011. Dynamic simulation of spur gear with tooth root crack propagating along tooth width and crack depth. Engineering Failure Analysis 18(8), 2149–2164.

[10] Chen, Z., Zhai, W., Shao, Y., Wang, K., 2016. Mesh stiffness evaluation of an internal spur gear pair with tooth profile shift. Science China Technological Sciences, 59(9), 1328–1339.

[11] Chen, Z., Zhou, Z., Zhai, W., Wang, K., 2020. Improved analytical calculation model of spur gear mesh excitations with tooth profile deviations. Mechanism and machine theory, 149, 103838 .

[12] Conry, T.F., Seireg, A., 1973. A Mathematical Programming Technique for the Evaluation of Load Distribution and Optimal Modifications for Gear Systems. Journal of Engineering for Industry 95, 1115–1122.

[13] Fernández, A., Iglesias, M., de Juan, A., García, P., Sancibrián, R., Viadero, F., 2014. Gear transmission dynamic: Effects of tooth profile deviations and support flexibility. Applied Acoustics 77, 138–149.

[14] Garambois, P., Perret-Liaudet, J., Rigaud, E., 2017. NVH robust optimization of gear macro and microgeometries using an efficient tooth contact model. Mechanism and Machine Theory 117, 78–95.

[15] Greenwood, J.A., Williamson, J.B.P., Bowden, F.P., 1966. Contact of nominally flat surfaces. Proceedings of the Royal Society of London. Series A. Mathematical and Physical Sciences 295(1442), 300–319. Royal Society.

[16] Guyan, R.J., 1965. Reduction of stiffness and mass matrices. AIAA Journal 3(2), 380-380.

[17] Harris, S.L., 1958. Dynamic Loads on the Teeth of Spur Gears. Proceedings of the Institution of Mechanical Engineers 172(1), 87-112.

[18] Houser, D.R., 1985. Gear Noise Sources and Their Prediction Using Mathematical Models. Gear Dynamics and Gear Noise Research Laboratory, Ohio State Univ.

[19] Houser, D.R., 2011. User's guide for the osu load distribution program (ldp), shaft analysis program, and rmc .

[20] Johnson, K.L., 1987. Contact Mechanics. Cambridge University Press.

[21] Kahraman, A., Blankenship, G.W., 1999. Effect of Involute Tip Relief on Dynamic Response of Spur Gear Pairs. Journal of Mechanical Design 121, 313–315.

[22] Kocak, S., Akay, H.U., Ecer, A., 1999. Parallel Implicit Treatment of Interface Conditions in Domain Decomposition Algorithms. In Parallel Computational Fluid Dynamics 1998 (pp. 353-360) , 353–360.

[23] Koffel, G., Ville, F., Changenet, C., Velex, P., 2009. Investigations on the power losses and thermal effects in gear transmissions. Proceedings of the Institution of Mechanical Engineers, Part J: Journal of Engineering Tribology, 223(3), 469-479 .

[24] Kurokawa, S., Ariura, Y., Ohtahara, M., 1996. Transmission errors of cylindrical gears under load - influence of tooth profile modification and tooth deflection. American Society of Mechanical Engineers, Design Engineering Division (Publication) DE 88, 213–217.

[25] Laursen, T.A., Maker, B.N., 1995. An augmented Lagrangian quasi-Newton solver for constrained nonlinear finite element applications. International Journal for Numerical Methods in Engineering 38(21), 3571–3590.
[26] Lin, T., He, Z., 2017. Analytical method for coupled transmission error of helical gear system with machining errors, assembly errors and tooth modifications. Mechanical systems and signal processing, 91, 167-182 , 167– 182.
[27] Mark, W.D., 2018. Tooth-meshing-harmonic static-transmission-error amplitudes of helical gears. Mechanical systems and signal processing, 98, 506-533 .
[28] Mohan, Y., Seshaiah, T., 2012. Spur Gear Optimization By Using Genetic Algorithm. International Journal Engineering Research and Applications 2(1), 311–318.
[29] Munro, R., Yildirim, N., Hall, D., 1990. Optimum profile relief and transmission error in spur gears. Gearbox noise and vibration , 35–42.
[30] Neufond, J., Denimal, E., Rigaud, E., Perret-Liaudet, J., Carbonelli, A., 2019. Whining noise computation of a planetary gear set induced by the multi-mesh excitations. Proceedings of the Institution of Mechanical Engineers, Part C: Journal of Mechanical Engineering Science 233(21-22), 7236 – 7245.
[31] Ničeno, B., Hanjalić, K., 2001. Large eddy simulation (LES) on distributed memory parallel computers using an unstructured finite volume solver. Parallel Computational Fluid Dynamics CFD 2000 Conference (p. 457), North-Holland .
[32] Opitz, H., Richards, E.J., 1968. A discussion on the origin and treatment of noise in industrial environments - Noise of gears. Philosophical Transactions of the Royal Society of London. Series A, Mathematical and Physical Sciences 263(1142), 369–380.
[33] Parker, R.G., Vijayakar, S.M., Imajo, T., 2000. Non-linear dynamic response of a spur gear pair: modelling and experimental comparisons. Journal of Sound and Vibration 237(3), 435–455.
[34] Perret-Liaudet, J., 1996. An original method for computing the response of a parametrically excited forced system. Journal of Sound and Vibration 196(2), 165–177.
[35] Petrov, E.P., Ewins, D.J., 2003. Analytical Formulation of Friction Interface Elements for Analysis of Nonlinear Multi-Harmonic Vibrations of Bladed Disks. J. Turbomach 125(2), 364–371.
[36] Portron, S., Velex, P., Abousleiman, V., 2019. A hybrid model to study the effect oftooth lead modifications on the dynamic behavior of double helical planetary gears. Proceedings of the Institution of Mechanical Engineers, Part C: Journal of Mechanical Engineering Science, 233(21–22) 7224–7235 .
[37] Rigaud, E., Barday, D., . Modelling and analysis of static transmission error. Effect of wheel body deformation and interactions between adjacent loaded teeth. Proceedings of the 4th World Congress on Gearing and Power Transmission, Paris, Vol. 3, 1999, pp.1961-1972 .
[38] Fernández-del Rincon, A., Iglesias, M., de Juan, A., Diez-Ibarbia, A., García, P., Viadero, F., 2016. Gear transmission dynamics: Effects of index and run out errors. Applied acoustics, 108 , 63– 83.
[39] Rémond, D., Velex, P., Sabot, J., 1993. Comportement dynamique et acoustique des transmissions par engrenages : synthèse bibliographique. p. 127, CETIM .
[40] Sainsot, P., Velex, P., Duverger, O., 2004. Contribution of gear body to tooth deflections - A new bidimensional analytical formula. J. Mech. Des., 126(4), 748–752.
[41] Salles, L., Staples, B., Hoffmann, N., Schwingshackl, C., 2016. Continuation techniques for analysis of whole aeroengine dynamics with imperfect bifurcations and isolated solutions. Nonlinear Dynamics 86(3), 1897–1911.
[42] Sánchez, M., Pleguezuelos, M., Pedrero, J.I., 2019. Influence of profile modifications on meshing stiffness, load sharing, and trasnsmission error of involute spur gears. Mechanism and machine theory 139, 506-525.
[43] Sauer, R.A., 2011. Enriched contact finite elements for stable peeling computations. International Journal for Numerical Methods in Engineering 87(6), 593–616.
[44] Savsani, V., Rao, R.V., Vakharia, D.P., 2010. Optimal weight design of a gear train using particle swarm optimization and simulated annealing algorithms. Mechanism and Machine Theory 45(3), 531–541.
[45] Simo, J.C., Laursen, T.A., 1992. An augmented lagrangian treatment of contact problems involving friction. Computers & Structures 42(1), 97-116.
[46] Singh, A., Houser, D.R., 1994. Analysis of off-line of action contact at the tips of gear teeth. SAE transactions 196-203.
[47] Suzuki, T., Umezawa, K., Houjoh, H., Bagiasna, K., 1987. Influence of Misalignment on Vibration of Helical Gear. JSME international journal: bulletin of the JSME, 30(259), 201.
[48] Szwedowicz, J., Kissel, M., Ravindra, B., Kellerer, R., 2001. Estimation of Contact Stiffness and its Role in the Design of a Friction Damper. In ASME Turbo Expo 2001: Power for Land, Sea, and Air. American Society of Mechanical Engineers Digital Collection .
[49] Tavakoli, M.S., Houser, D.R., 1986. Optimum Profile Modifications for the Minimization of Static Transmission Errors of Spur Gears. Journal of Mechanisms, Transmissions, and Automation in Design 108, 86–94.
[50] Ulaga, S., Ulbin, M., Flašker, J., 1999. Contact problems of gears using Overhauser splines. International Journal of Mechanical Sciences 41(4), 385–395.
[51] Umezawa, K., Sato, T., Ishikawa, J., 1984. Simulation of rotational vibration of spur gear. Bulletin of JSME, 27(223), 102-109. .
[52] Umezawa, M., 1995. Effects of deviation of tooth surface errors of a helical gear pair on the transmission Eerror. Transactions of the Japan Society of Mechanical Engineers Series C 61, 3101–3107.
[53] Velex, P., Ville, F., 2009. An Analytical Approach to Tooth Friction Losses in Spur and Helical Gears—Influence of Profile Modifications. Journal of Mechanical Design 131(10).
[54] Vijayakar, S.M., 1991. A combined surface integral and finite element solution for a three-dimensional contact problem. International Journal for Numerical Methods in engineering, 31(3), 525-545 .
[55] Vinayak, H., Singh, R., Padmanabhan, C., 1995. Linear dynamic analysis of multi-mesh transmissions containing external, rigid gears. Journal of Sound and Vibration 185(1), 1–32.
[56] Wang, C., 2021. Multi-objective optimal design of modification for helical gear. Mechanical systems and signal processing 157, 107763.
[57] Welbourn, D.B., 1979. Fundamental knowledge of gear noise: a survey. No. IMechE-C117/79.

[58] Wriggers, P., 2006a. Discretization, Large Deformation Contact. Computational Contact Mechanics (pp. 225-307). Springer, Berlin, Heidelberg .
[59] Wriggers, P., 2006b. Discretization of the Continuum. In Computational Contact Mechanics (pp. 157-182). Springer, Berlin, Heidelberg .
[60] Wriggers, P., 2006c. Discretization, Small Deformation Contact. Computational Contact Mechanics (pp. 183-224). Springer, Berlin, Heidelberg .
[61] Wriggers, P., 2006d. Introduction to Contact Mechanics. Computational Contact Mechanics (pp. 11-29). Springer, Berlin, Heidelberg .
[62] Xiang, L., Gao, N., 2017. Coupled torsion–bending dynamic analysis of gear-rotor-bearing system with eccentricity fluctuation. Applied Mathematical Modelling 50, 569–584.
[63] Yang, D.C.H., Lin, J.Y., 1987. Hertzian Damping, Tooth Friction and Bending Elasticity in Gear Impact Dynamics. Journal of Mechanisms, Transmissions, and Automation in Design 109, 189–196.
[64] Yonekawa, K., Kawahara, M., 2001. Analysis of Tidal Flow Using Kalman Filter Finite Element Method with Domain Decomposition Method. In Computational Mechanics–New Frontiers for the New Millennium (pp. 155-160). Elsevier .
[65] Yuruzume, I., Mizutani, H., Tsubuku, T., 1979. Transmission Errors and Noise of Spur Gears Having Uneven Tooth Profile Errors. Journal of Mechanical Design 101, 268–273.
[66] Özgüven, H., Houser, D.R., 1988. Mathematical models used in gear dynamics—A review. Journal of Sound and Vibration 121(3), 383–411.

CRediT authorship contribution statement

Y. Benaïcha: Conceptualization, Methodology, Software, Validation, Investigation, Writing - Original Draft, Writing - Review and Editing, Visualization. **J. Perret-Liaudet:** Conceptualization,Supervision, Funding acquisition, Writing - Review and Editing. **J-D. Beley:** Conceptualization,Supervision, Funding acquisition, Writing - Review and Editing. **E. Rigaud:** Supervision,Writing - Review and Editing. **F. Thouverez:** Conceptualization,Supervision, Funding acquisition, Writing - Review and Editing.